JOURNAL OF GEOPHYSICAL RESEARCH, VOL. 103, NO. A2, PAGES 2377–2383, FEBRUARY 1, 1998

MHD wave coupling in the geomagnetic tail with field-aligned density variations

Andrew N. Wright and Andrew R. Garman

Mathematical Institute, University of St. Andrews, Fife, Scotland

Abstract. The normal MHD modes of the tail lobe are calculated for a simple model that is stratified in z. An important feature of our equilibrium field is that it may be tilted at an arbitrary angle (θ) to the antisunward direction, i.e., $\mathbf{B} = B(\cos\theta, 0, \sin\theta)$. When $\theta = 0$, the familiar singular second-order equation of *Southwood* [1974] is recovered. When $\theta \neq 0$, the system is goverened by a nonsingular fourth-order equation. *Hansen and Harrold* [1994] (hereafter HH) considered exactly this system and concluded that (for $\theta \neq 0$) energy was no longer absorbed by a singularity but rather over a thickened boundary layer across which the time-averaged Poynting flux ($\langle S_z \rangle$) changed. Our results are not in agreement with those of HH. We find $\langle S_z \rangle$ is independent of z and find no evidence of boundary layers, even for θ as small as 10^{-6} rad. Our solutions still demonstrate strong mode conversion from fast to Alfvén modes at the "resonant" position, but the small component of Alfvén speed in the $\hat{\mathbf{z}}$ direction permits the Alfvén waves to transport energy away from this location and prevents the continual accumulation of energy there. The implications for MHD wave coupling in realistic tail equilibria are discussed.

1. Introduction

Large-scale reconfigurations of the geomagnetic tail from internal or external driving mechanisms are described naturally in terms of MHD waves. Recently, *Elphinstone et al* [1995] observed the clear signature of a fast magnetosonic wave in the magnetometer data of IMP 8 recorded in the tail lobe. There is also a long history of studying the normal modes of the tail, and it is thought that these can account for Pi 2s [*Edwin et al.*, 1986; *Hopcraft and Smith,* 1986].

Detailed studies of magnetotail modes frequently assume an equilibrium field $B(z)\hat{\mathbf{x}}$ and a harmonic dependence on the x and y (GSE) coordinates, which reduces the normal mode equations to a second-order ordinary differential equation (ODE) in z. Formally, these equations are similar to the singular field line resonance equations of *Southwood* [1974] and *Chen and Hasegawa* [1974], which describe wave coupling on closed field lines. *Seboldt* [1990] and *Liu et al.* [1995] have calculated these normal modes, which describe MHD wave coupling on open tail field lines.

Recently, *Hansen and Harrold* [1994] (hereafter HH) have argued that the one-dimensional equilibrium used in all these previous studies (in which $\hat{\mathbf{x}}B$ and ρ are solely functions of z) is unrealistic, since there must be some, albeit small, variation of ρ along the equilibrium field lines. HH proposed a modified equilibrium (see Figure 1) in which $\rho(z)$ is still a function of z, but the equilibrium field is tilted so that it has a small z component $\mathbf{B} = (B_x, 0, B_z)$. Even for the simple case of $\mathbf{B}$ = const, $(\mathbf{B} \cdot \nabla)\rho = B_z(\partial\rho/\partial z)$ will be nonzero, and HH claim that this condition removes the Alfvén singularity even if B_z is very small. They go on to show that the energy deposition now occurs continuously over a thickened layer rather than at a singularity and is qualitatively unaffected from the singular ($B_z = 0$) case. We find this conclusion peculiar: A one-dimensional solution of the ideal equations with oscillatory time dependence and no singularities should have a time-averaged energy flux in the z direction that is independent of z – a property that is clearly violated in Figures 4 and 8 of HH.

We have performed our own analytical and numerical investigations of the system in Figure 1 and find that (1) there is no Alfvén singularity even as $B_z \to 0^+$ (it needs to be identically zero to get a singularity); (2) there is no energy accumulation in a layer centered on the $B_z = 0$ singularity as $B_z \to 0^+$; (3) the z component of the energy flux is independent of z; and (4) the $B_z = 0$ singularity marks an important position where an incoming fast wave can couple efficiently to an Alfvén wave. However, the Alfvén wave propagates along $\mathbf{B}$ and away from this z position when $B_z \neq 0$, thus preventing a continual accumulation of energy there.

It is interesting to note that if perfectly reflecting line-tied boundary conditions were employed in the x direction, such as on closed field lines, the resulting partial

Paper number 97JA02865.
0148-0227/98/97JA-02865$09.00

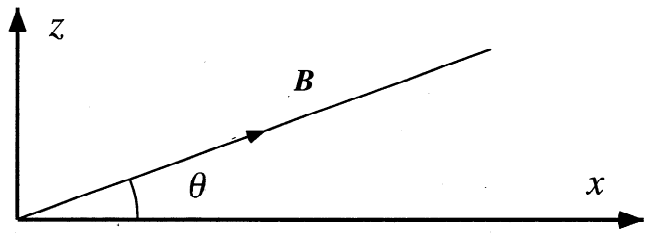

Figure 1. Model equilibrium and coordinates. The magnetic field $\mathbf{B} = B(\cos\theta, 0, \sin\theta)$ has constant strength. The density varies only with z, so if θ is nonzero there is a field-aligned density variation.

differential equations in x and z would be singular even when $B_z \neq 0$ [*Thompson and Wright*, 1993]. In this case, each field line has a well-defined set of natural Alfven frequencies.

2. Model and Governing Equations

For simplicity, and to facilitate direct comparison with the results of HH, we take $\mathbf{B}$ to be constant and inclined at an angle θ to the $\hat{\mathbf{x}}$ direction (see Figure 1). The density is solely a function of z,

$$\mathbf{B} = B(\cos\theta, 0, \sin\theta) \tag{1}$$

$$\rho = \rho(z) \tag{2}$$

and we neglect plasma pressure, so the model equilibrium could describe low-β regions of the tail lobe or possibly the plasma sheet boundary layer.

For an ideal plasma the linear MHD perturbations to the plasma velocity ($\mathbf{u}$) and magnetic field ($\mathbf{b}$) are governed by the momentum equation

$$\rho\frac{\partial \mathbf{u}}{\partial t} = (\nabla\wedge\mathbf{b})\wedge\mathbf{B}/\mu_0 \tag{3}$$

and the induction equation

$$\frac{\partial \mathbf{b}}{\partial t} = \nabla\wedge(\mathbf{u}\wedge\mathbf{B}) \tag{4}$$

Considering a single Fourier mode $\exp i[k_x x + k_y y - \omega t]$ reduces (3) and (4) to a set of ODEs in z. If we write d/dz as a prime, the components of (3) and (4) become

$$\begin{aligned} b_x' &= B\sec\theta\left[\frac{i\omega}{V^2} - \frac{ik_x^2}{\omega}\right]u_z \\ &\quad + \sin\theta\frac{ik_xk_yB}{\omega}u_y \end{aligned} \tag{5a}$$

$$\begin{aligned} b_y' &= \sin\theta\frac{ik_y^2B}{\omega}u_y - \csc\theta\frac{i\omega B}{V^2}u_y \\ &\quad - \sec\theta\frac{ik_xk_yB}{\omega}u_z + ik_y\cot\theta b_x \\ &\quad - ik_x\cot\theta b_y \end{aligned} \tag{5b}$$

$$u_y' = -\csc\theta\frac{i\omega}{B}b_y - ik_x\cot\theta u_y \tag{5c}$$

$$u_z' = \cos\theta\frac{i\omega}{B}b_x - ik_y\cos^2\theta u_y \tag{5d}$$

In the above equations, V is the Alfvén speed ($V^2 = B^2/\mu_0\rho$), and we have eliminated b_z and u_x as they are determined algebraically,

$$u_x = -\tan\theta u_z \tag{6a}$$

$$\begin{aligned} \frac{b_z}{B} &= -\frac{k_x}{\omega}\cos\theta u_z + \frac{k_x}{\omega}\sin\theta u_x \\ &\quad + \frac{k_y}{\omega}\sin\theta u_y \end{aligned} \tag{6b}$$

Note that the wave fields in (5) and (6) are complex, having nonzero real and imaginary parts.

3. Singularities

To identify the existence, or absence, of singularities in the solution to (5), we write these equations as a single fourth-order ODE. Singularities may occur when the coefficient of the highest derivative vanishes. To ease comparison with HH, we write the equation in their notation and work with plasma displacement in the z direction; $\xi_z \equiv iu_z/\omega$. The resulting equation is

$$A_4\xi_z'''' + A_3\xi_z''' + A_2\xi_z'' + A_1\xi_z' + A_0\xi_z = 0 \tag{7}$$

The coefficients are given by

$$A_4 = \eta^4 + \eta^2 \tag{8a}$$

$$A_3 = (\eta^4 + \eta^2)S'/\tilde{A} + 2ik_x(\eta^3 + \eta) \tag{8b}$$

$$\begin{aligned} A_2 &= \eta^4k_x^2 + 2iS'\eta k_x/\tilde{A} + S + \eta^6k_x^2 \\ &\quad -\eta^2\tilde{A} + i\eta^5k_xS'/\tilde{A} + \eta^2R \\ &\quad +k_y^2 + 3i\eta^3k_xS'/\tilde{A} \end{aligned} \tag{8c}$$

$$\begin{aligned} A_1 &= -2i\eta^3k_xk_y^2 - 2i\eta k_xk_y^2 - S'\eta^4k_x^2/\tilde{A} \\ &\quad +k_y^2S'/\tilde{A} + 2i\eta k_xR + 2\eta^2R' \\ &\quad +\eta^2k_y^2S'/\tilde{A} - 2i\eta^3k_x^3 + S'\eta^2R/\tilde{A} \end{aligned} \tag{8d}$$

$$\begin{aligned} A_0 &= \eta^2R'' + \eta^4k_x^2R - \eta^6k_x^4 + 2\eta^2k_x^2R \\ &\quad +2i\eta k_xR' - \eta^2k_x^2k_y^2 + iS'\eta^3k_xR/\tilde{A} \\ &\quad -ik_y^2k_x\eta S'/\tilde{A} + \tilde{A}\eta^2k_x^2 - 2ik_x^3\eta^3S'/\tilde{A} \\ &\quad +S'\eta R'/\tilde{A} - iS'\eta^5k_x^3/\tilde{A} - 2\eta^4k_x^4 \\ &\quad -ik_y^2\eta^3k_xS'/\tilde{A} + 2iS'\eta k_xR/\tilde{A} \\ &\quad -\tilde{A}R - \eta^4k_x^2k_y^2 \end{aligned} \tag{8e}$$

where a common multiplicative factor of $\tilde{A} = \eta^2k_y^2 + 2\eta^2k_x^2 + \eta^4k_x^2 - S$ has been omitted from all coefficients in (8). The following quantities are defined by HH: $R = \omega^2/V_{Ax}^2 - k_x^2$, $S = \omega^2/V_{Ax}^2 - k_x^2 - k_y^2$, and $V_{Ax}^2 = B_{0x}^2/(\mu_0\rho)$. Note that HH took $\mathbf{B} = B_{0x}(1, 0, \eta)$, so the results may be converted to our notation by substituting $B_{0x} \equiv B\cos\theta$ and $\eta = \tan\theta$.

It is a tedious task to derive the coefficients in (8) without approximations or dropping terms. Indeed, HH focused on the small θ (or η) limit and omitted many

of the higher-order terms (see their equation (19)). We employed Maple to derive the result in (8), which is valid for arbitrary θ. We were also able to check our result by recovering the constant density (arbitrary θ) limit, which reduces (7) to the fast and Alfvén dispersion relations.

As we noted above, any singularities will occur when the coefficient of the highest derivative is zero. This condition is not satisfied for a special value of z but is achieved by setting θ (or η) to zero exactly. When $\theta = 0$ we find $A_4 = A_3 = 0$ identically, and (7) is reduced to the familiar second-order ODE of *Southwood* [1974]. The Alfvén singularities of this equation are well documented. Note that this system has constant ρ along field lines. If we wish to study equilibria for which ρ varies along $\mathbf{B}$, then θ (and η) must be nonzero, and so A_4 will never vanish indicating that there is no singularity in the fourth-order ($\theta \neq 0$) equation. HH also reached this conclusion. However, as the coefficients of the highest derivatives (A_3 and A_4) will be small when θ is small, they suggested that a boundary layer solution would be appropriate and found that energy could be deposited in the boundary layer. We find this claim surprising, and in the following sections we develop what we believe to be the correct solution.

4. Analytical and Numerical Solutions

To develop some understanding of the wave modes in the nonuniform equilibrium, we begin by considering the limit in which $k_y = 0$. This simplification decouples the Alfvén wave (characterized by b_y and u_y) from the fast mode (b_x, b_z, u_x, u_z).

4.1. Decoupled Solutions

A WKB solution may be determined for the field-guided Alfvén perturbations. The length scale of the field-aligned density variation (L) is given by $1/L = (\mathbf{B}/B)\cdot\nabla \ln\rho = \sin\theta d(\ln\rho)/dz$ and may be made arbitrarily large by choosing θ sufficiently small. The parallel wavelength of the Alfvén wave ($2\pi/k_\parallel$) is determined by the local dispersion relation $k_\parallel^2(z) = \omega^2/V^2(z)$, where $V(z)$ is the Alfvén speed. Provided that $k_\parallel^2 \gg 1/L^2$, a WKB solution can (normally) be employed, and this can generally be satisfied for small θ. (Strictly, we require $k_z \gg 1/L_z$, as we are solving equations in z only; see later.)

A WKB solution assumes a dependence on z of $\exp i[k_z(z)z]$. Setting $k_y = 0$ and replacing d/dz by ik_z in equations (5) yield the following equation for the Alfvén wave:

$$\begin{pmatrix} -k_x\cot\theta & -\omega/(B\sin\theta) \\ -\omega B/(V^2\sin\theta) & -k_x\cot\theta \end{pmatrix}\begin{pmatrix} u_y \\ b_y \end{pmatrix} = k_z\begin{pmatrix} u_y \\ b_y \end{pmatrix} \quad (9)$$

which is an eigenvalue equation for k_z. The roots are

$$k_z^\pm = (\pm\frac{\omega}{V} - k_x\cos\theta)/\sin\theta \quad (10)$$

That these roots correspond to the Alfvén wave may be confirmed by calculating $k_\parallel$:

$$k_\parallel^\pm = k_x\cos\theta + k_z^\pm\sin\theta \equiv \pm\omega/V \quad (11)$$

so $k_\parallel^2$ does indeed satisfy the Alfvén wave dispersion relation. Clearly the +/− roots correspond to propagation parallel/antiparallel to $\mathbf{B}$. This property is also evident from the eigenvectors of (9),

$$k_z = k_z^+;\ \ (u_y, b_y) = a(z)(1, -B/V) \quad (12a)$$

$$k_z = k_z^-;\ \ (u_y, b_y) = a(z)(1, +B/V) \quad (12b)$$

where $a(z)$ is some arbitrary function of z for the moment. The result in (12) that $b_y/u_y = +/- B/V$ for an Alfvén wave propagating antiparallel/parallel to $\mathbf{B}$ is also familiar.

A graphical interpretation of the wavevector (eigenvalue) is instructive. Figure 2 shows the solution in (k_x, k_z) space. Consider Figure 2a first. Our solution has a prescribed k_x, which is marked by the vertical dashed line. The wave vector must have an x component equal to this k_x, and so its tip will lie on the vertical dashed line. The z component of $\mathbf{k}$ may be determined from the Alfvén wave dispersion relation, $k_\parallel = \pm\omega/V$, and the two tilted dashed lines delineate this constraint. The two points of intersection of the lines represent our solution for $\mathbf{k}^+$ and $\mathbf{k}^-$. Evidently, their projection onto the field-aligned direction will yield a $k_\parallel$ that satisfies the Alfvén wave dispersion relation.

Regarding (10), we see that k_z^- is always negative, as is $k_\parallel^-$. Thus the phase velocity and group velocity of the $\mathbf{k}^-$ solution are always in the $-\mathbf{z}$ direction. The $\mathbf{k}^+$ solution is more unusual, and from (10) we see that $k_z^+ = 0$ when

$$\frac{\omega}{V(z)} = k_x\cos\theta \quad (13)$$

This condition is satisfied for some special value of z (assuming V and ρ vary monotonically). Note that when θ is zero, (13) defines the position z_r (the location of the resonant Alfvén wave singularity). When θ is nonzero, (13) defines a critical position (z_c) which is approximately equal to z_r for small θ,

$$z_c = z_r + O(\theta^2) \quad (14)$$

Since k_z^+ changes sign across $z = z_c$, the phase velocity in the z direction ($V_p^+ = \omega/k_z^+$) also changes sign. (This behavior is quite different to $V_p^- = \omega/k_z^-$, which is always negative.) A graphical view is given in Figure 2: in Figure 2a $k_z^+ > 0$, so $\omega/V(z) > k_x\cos\theta$. This inequality is satisfied for z values where $\rho(z) > \rho(z_c)$. The situation $\rho(z) < \rho(z_c)$ is shown in Figure 2b, from which it is clear that k_z^+ is negative.

The group velocity can be determined from rewriting (10) as

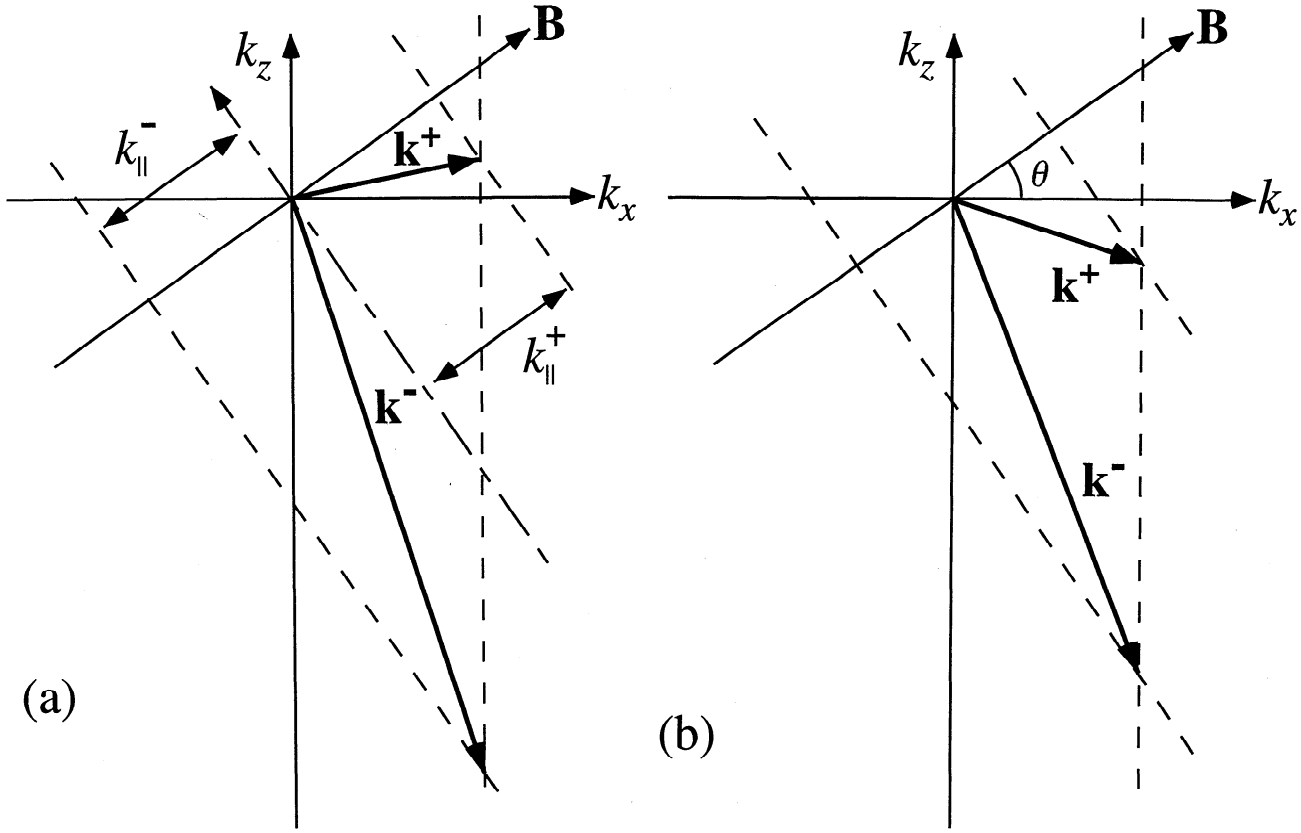

Figure 2. Graphical Alfvén wave solution in $(k_x, k_y = 0, k_z)$ wavenumber space. The normal mode has a prescribed k_x (vertical dashed line) and ω. The parallel wave numbers are found from $k_\parallel^2 = \omega^2/V_A^2(z)$ and so must lie on the tilted dashed lines. The roots correspond to the points of intersection of these lines. The sign of k_z^+ changes sign according to whether $V(z)$ is (a) smaller than or (b) larger than $\omega/(k_x \cos\theta)$.

$$\omega = \pm(k_z^\pm \sin\theta + k_x \cos\theta)V \tag{15}$$

from which we find the z component of the group velocity,

$$V_g^\pm = \frac{\partial\omega}{\partial k_z^\pm} = \pm V \sin\theta \tag{16}$$

Thus the group velocity is parallel/antiparallel to **B** for the +/− solutions and has a magnitude equal to the component of the Alfvén speed in the $\hat{\mathbf{z}}$ direction. Employing (15) and (16), we find the ratio of the z components of group and phase velocities is

$$\frac{V_g^\pm}{V_p^\pm} = 1 \mp \frac{k_x V}{\omega} \cdot \cos\theta \tag{17}$$

Hence the k_z^- solution (i.e., taking the lower sign in (17)) always has V_g^- parallel to V_p^- (both negative). The k_z^+ solution has V_g^+ parallel to V_p^+ when $\rho(z) > \rho(z_c)$, $(V(z) < V(z_c))$, and they are of opposite sense when $\rho(z) < \rho(z_c), (V(z) > V(z_c))$. This behavior is a result of V_p^+ (and k_z^+) changing sign at z_c.

To illustrate further features of these solutions, we turn to a numerical solution. In all the numerical solutions, normalized quantities are employed. Length is normalized by the extent of the domain (l) in z, velocities by $V(0)$, density by $\rho(0)$, magnetic field strength by $B(0)$, and time by $l/V(0)$. The model density and Alfvén speed on the normalized interval $0 < z < 1$ are

$$\rho = (10z^4 + 1)^2; \qquad V = \frac{1}{10z^4 + 1} \tag{18}$$

The normalized version of (5) is solved by specifying boundary conditions at $z = 0$ and then integrating with a fourth-order Runge-Kutta scheme to $z = 1$. In all the results presented here, 8000 grid points in z were used, and this resolution determined the solution fields to 1 part in 10^6.

Figure 3 (top) was generated by applying the k_z^+ eigenvector $(u_{yr}, b_{yr}) = (1, -1)$ at $z = 0$, whereas Figure 3 (bottom) used the k_z^- eigenvector $(u_{yr}, b_{yr}) = (1, 1)$ as a boundary condition. (Other parameters were $k_x = 3.0$, $k_y = 0.0$, $\omega = 1.0$, and $\theta = 0.03$ rad.) The point where k_z^+ changes sign for this model is $z_c = 0.669$, and is indicated by the dashed line in Figure 3. Indeed, at this position $\lambda_z^+ = 2\pi/k_z^+$ is locally very large. We can go further and compare $\lambda_z^\pm$ with the wavelengths in Figure 3. For example, $\lambda_z^+(0) = -0.094$, $\lambda_z^+(1) = 0.024$, $\lambda_z^-(0) = -0.047$, and $\lambda_z^-(1) = -0.014$. A careful examination shows that these WKB wave-

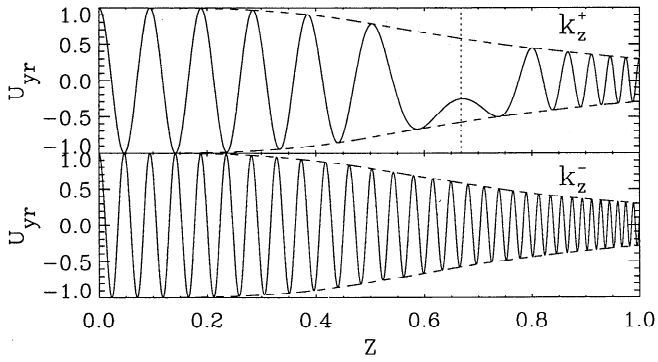

Figure 3. Decoupled Alfvén wave eigenfunctions: (top) k_z^+ and (bottom) k_z^-. The dashed lines represent the WKB amplitude envelope $\propto \rho^{-1/4}$.

length estimates are in excellent agreement with the numerical results. The ratio of λ_z^- to λ_z^+ is easily calculated from (10),

$$\frac{\lambda_z^-}{\lambda_z^+} = \frac{k_z^+}{k_z^-} = \frac{1-\cos\theta k_x V/\omega}{-1-\cos\theta k_x V/\omega} \tag{19}$$

so $\lambda_z^-/\lambda_z^+ \to 0$ as $z \to z_c$. The following limits are also found:

$$\frac{\lambda_z^-}{\lambda_z^+} \to -1; \qquad V(z) \ll V(z_c) \tag{20a}$$

$$\frac{\lambda_z^-}{\lambda_z^+} \to +1; \qquad V(z) \gg V(z_c) \tag{20b}$$

The trend toward these limits is also visible in Figure 3. ($V(0)/V(z_c) = 3.0$, $V(1)/V(z_c) = 0.273$.) The lowest-order WKB solution developed so far (geometrical optics) determines the phase of the solution. It is evident from the numerical solution that the amplitude also varies, and this may be analyzed by solving the next order of the WKB equations (physical optics). Physical optics has the advantage that the solution amplitude satisfies energy conservation. We can use this as a shortcut to deduce the amplitude variation; in a constant magnetic field the Poynting vector is proportional to $u_y b_y$, and this must be constant, as the (small wavelength) wave suffers no reflection. Since $u_y = \pm b_y(V/B)$, we find $u_y \propto \rho^{-1/4}$ and $b_y \propto \rho^{1/4}$. The amplitude envelope $\rho^{-1/4}$ is shown in Figure 3 and is an excellent approximation, except near z_c for the k_z^+ solution, where $\lambda_z^+ \to \infty$ and the WKB ordering discussed earlier is violated. Hence the previously unspecified amplitude $a(z)$ of the eigenvectors in (12) is now determined to be $a(z) \propto \rho^{-1/4}(z)$.

4.2. Coupled Solutions

When $k_y = 0$ (such as in Figure 3), the decoupled Alfvén waves carry constant (time-averaged) energy flux. The k_z^+/k_z^- solution carries a flux in the $+/-\hat{\mathbf{z}}$ direction. When $k_y \neq 0$, the Alfvén waves couple to the fast mode; both real and imaginary parts of the four complex ODEs in (5) become coupled together. Although we solve for all these coupled components numerically, for the purposes of studying the solutions it is sufficient to plot u_{yr} and u_{zr} (the real parts of u_y and u_z), which represent the Alfvén and fast modes, respectively.

In Figure 4 we plot $u_{yr}(z)$ and $u_{zr}(z)$ for $k_x = 3.0$, $k_y = 1.0$, $\omega = 1.0$, and $\theta = 0.03$ rad. The boundary conditions at $z = 0$ are $(u_{yr}, u_{zr}, b_{xr}, b_{yr}) = (0.2, 0.1, 0.0, -0.2)$ and $(u_{yi}, u_{zi}, b_{xi}, b_{yi}) = (0.0, 0.0, -0.1, 0.0)$. The λ_z^+ scale seen in Figure 3 is evident in this figure, but note how the amplitude envelope of the u_{yr} is discontinuous. (We have overplotted portions of the WKB envelope, scaled suitably, on either side of z_c.) The energy flux carried by the Alfvén wave over the range $0 < z < 0.5$ is evidently much less than that carried over the section $0.8 < z < 1.0$. Where does the extra energy come from? The time-averaged z component of the Poynting vector is shown in the bottom panel and is calculated from

$$\begin{aligned}\langle S_z \rangle &= -\tfrac{1}{2} Re\,\{(\mathbf{u}\wedge\mathbf{B})\wedge\mathbf{b}\}\cdot\hat{\mathbf{z}} \\ &= \tfrac{1}{2}[u_{zr}b_{xr}B_x - u_{xr}b_{xr}B_z - u_{yr}b_{yr}B_z \\ &\quad + u_{zi}b_{xi}B_x - u_{xi}b_{xi}B_z - u_{yi}b_{yi}B_z]\end{aligned} \tag{21}$$

(Re indicating the real part). As there are no singularities in our ideal equations, we would expect $\langle S_z \rangle$ to be independent of z, and Figure 4 is in accord with this. (Numerically, $\langle S_z \rangle$ was constant to 11 significant figures.) Our results are in contradiction with the nu-

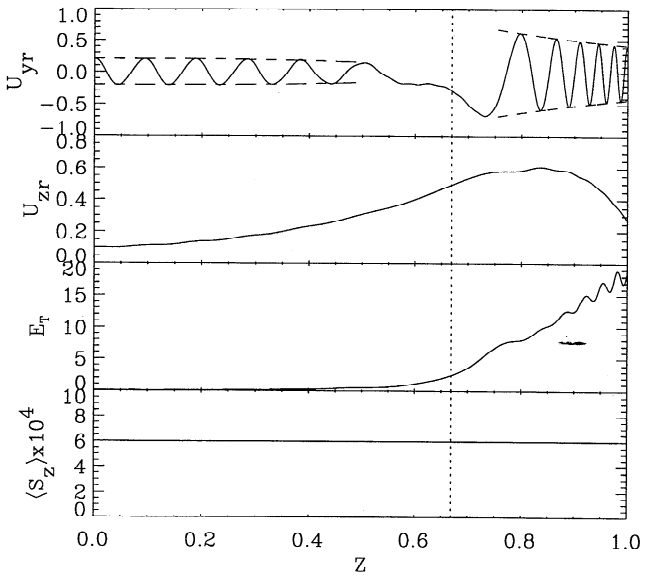

Figure 4. Variation of u_{yr} (Alfvén wave), u_{zr} (fast mode), time-averaged total energy density, and time-averaged z component of the Poynting vector. The dashed vertical line marks the position z_c where $V(z_c) = \omega/(k_x \cos\theta)$. Note that $\langle S_z \rangle$ is independent of z. (Here, $k_x = 3.0$, $k_y = 1.0$, $\omega = 1.0$, $\theta = 0.03$; at $z = 0$ $(u_{yr}, u_{zr}, b_{xr}, b_{yr}) = (0.2, 0.1, 0.0, -0.2)$, and $(u_{yi}, u_{zi}, b_{xi}, b_{yi}) = (0.0, 0.0, -0.1, 0.0)$.)

merical results of HH (their Figures 4 and 8) who found that $\langle S_z \rangle$ varied by the order of 100%.

Not only does $\langle S_z(z) \rangle$ show a complete absence of an energy absorption signature near z_c, but the time-averaged total energy density (E_T) (also displayed in Figure 4) shows no remarkable features or accumulation of energy around this position. In normalized units,

$$E_T = \frac{1}{4}\mathbf{b} \cdot \mathbf{b}^* + \frac{1}{4}\rho \mathbf{u} \cdot \mathbf{u}^* \qquad (22)$$

(where the asterisk denotes the complex conjugate). Note that in (21) and (22) the fields are the Fourier coefficients, which are solely a function of z.

The second panel in Figure 4 shows the variation of u_{zr} with z and. to a good approximation, describes the fast mode. The turning point near z_c is the demarcation line between the oscillatory ($z_c < z < 1$) and evanescent ($0 < z < z_c$) regions. We noted above that the time-averaged flux associated with the Alfvén wave is not independent of z, since the amplitude of the WKB envelope is different on either side of z_c. However, the $\langle S_z \rangle$ panel demonstrates that total enegy flux (of the Alfvén and fast wave) is constant. The obvious interpretation is that the fast mode has a negative $\langle S_z \rangle$ in the region $z_c < z < 1$ but mode converts to an Alfvén wave propagating in the positive $\hat{\mathbf{z}}$ direction at $z \approx z_c$. Hence the Alfvén wave energy flux in the region $z_c < z < 1$ is greater than that in $0 < z < z_c$.

To confirm our interpretation of fast Alfvén wave coupling, we modified the boundary conditions to $(u_{yr}, u_{zr}, b_{xr}, b_{yr}) = (0.0, 0.15, 0.0, 0.0)$ and $(u_{yi}, u_{zi}, b_{xi}, b_{yi}) = (0.0, 0.0, -0.05, 0.0)$. As before, $k_x = 3.0$, $k_y = 1.0$, $\omega = 1.0$, and $\theta = 0.03$. The boundary conditions correspond to $\langle S_z \rangle = 0$ (from (21)), and the numerical solution shown in Figure 5 verifies this property. Moreover, at $z = 0$ the boundary conditions contain no Alfvén wave eigenvector (for k_z^+ or k_z^- solutions) but do contain an evanescent fast mode. The u_{yr} and u_{zr} panels confirm these features in the region $0 < z < z_c$. For $z_c < z < 1$ the solution is quite different. An Alfvén wave with λ^+ scale (i.e., carrying energy in the $+\hat{\mathbf{z}}$ direction) exists. Since $\langle S_z \rangle = 0$, the fast mode in $z_c < z < 1$ must be carrying energy from $z = 1$ to around z_c, where it converts to an Alfvén wave propagating from z_c to larger z. Although there is no singularity in the equations when $\theta \neq 0$, there is still efficient mode coupling between fast and Alfvén waves near $z = z_c$.

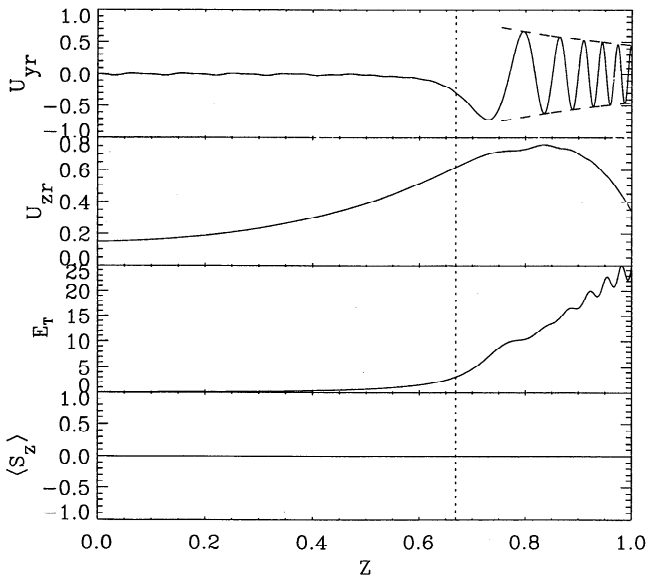

Figure 5. Same format and parameters as in Figure 4. The boundary conditions at $z = 0$ are $(u_{yr}, u_{zr}, b_{xr}, b_{yr}) = (0.0, 0.15, 0.0, 0.0)$ and $(u_{yi}, u_{zi}, b_{xi}, b_{yi}) = (0.0, 0.0, -0.05, 0.0)$. In the region $z_c < z < 1$ a fast mode propagates from $z = 1$ to $z = z_c$, where it mode converts to an Alfvén wave which propagates from $z = z_c$ to $z = 1$. There is no net time-averaged energy flux in the z direction.

5. Summary

In summary, we have investigated fast and Alfvén wave coupling for the HH equilibrium, which corresponds to that employed by *Southwood* [1974] except that the background magnetic field is confined to the (x, z) plane and allowed to tilt at an arbitrary angle θ to $\hat{\mathbf{z}}$.

1. When $\theta = 0$, the system is governed by the familiar singular field line resonance equation of *Southwood* [1974]. There is a singularity at z_r, $\omega^2 = k_x{}^2 V^2(z_r)$, and (for $k_y \neq 0$) a jump in $\langle S_z \rangle$ across z_r.

2. If θ is not identically zero, there is no singularity, no jump in $\langle S_z \rangle$, and no accumulation of energy evident in our solutions. (We even determined numerical solutions for $\theta = 10^{-6}$ rad and found no qualitative difference from the results shown in Figures 4 and 5.)

3. Strong mode coupling does occur between fast and Alfvén waves around z_c, but because the Alfvén speed has a small component in the $\hat{\mathbf{z}}$ direction, the Alfvén wave energy is not trapped at z_c.

It is interesting to consider why the $\theta = 0$ (singular) solution is so different from the $\theta \neq 0$ (nonsingular) solution, even when $\theta \to 0^+$. Mathematically, the difference arises because the two cases ($\theta = 0$, and $\theta \neq 0$) are governed by a singular second-order ODE and a nonsingular fourth-order ODE, respectively. Physically, the difference can be understood by considering the continual coupling of fast energy to Alfvén waves at $z = z_c$: Once the Alfvén waves have been excited, they propagate along the equilibrium field. If $\theta = 0$, the Alfvén waves propagate in x but remain at $z = z_c$; thus the Alfvén wave energy density increases in time at this position and manifests itself in a normal mode as a singularity. If $\theta \neq 0$, the Alfvén waves may propagate in x but also in z (at a speed $V \sin\theta$). Even when θ is small, the Alfvén waves' ability to propagate away from z_c prevents an accumulation of energy there, and no singularity results. Note that a normal mode with

real frequency has, in principle, existed for an indefinite time, so even a small Alfvén speed component in $\hat{\mathbf{z}}$ will have allowed the Alfvén waves to propagate to $z = \pm\infty$ (unless $V(z) \rightarrow 0$ for some z).

The implications of this study for wave coupling in the tail are that fast and Alfvén wave coupling will still occur if $\theta \neq 0$, but it is a little difficult to interpret normal mode solutions (which oscillate indefinitely) with realistic time-dependent behavior in a detailed manner. Naively, it seems reasonable that if wave coupling has been taking place for a time (t_0) such that the distance propagated by Alfvén waves in the $\hat{\mathbf{z}}$ direction ($\Delta z = V t_0 \sin\theta$) is much less than the phase mixing length ($L_{ph} = 2\pi/(t_0 d\omega_A/dz)$; $\omega_A \approx k_x V_A(z)$), then energy is still confined to around z_c, and the width of the "resonance" (L_{ph}) is sufficiently broad that the third- and fourth-order derivatives in (7) will be negligible. In this limit the tilt of the field is insignificant, and the solution should be similar to the untilted time-dependent calculations [e.g., *Mann et al.*, 1995].

For longer times when $\Delta z \gg L_{ph}$ the tilt of the field can not be neglected, and the solution should be asymptoting to the normal modes described here. Future work will calculate the time-dependent behavior of this system numerically and confirm the precise nature of the solutions in different regimes. It should then be possible to assess the significance of the nonsingular normal modes for describing wave coupling in the magnetotail.

Acknowledgments. A.N.W. is supported by a PPARC Advanced Fellowship and is grateful to PPARC and NIWA for funding his visit to the National Institute of Water and Atmospheric Research, where this work was completed. A.R.G. was supported by an EPSRC studentship. The authors are grateful to W. Allan for useful discussions.

The Editor thanks one referee for his assistance in evaluating this paper.

References

Chen, L., and A. Hasegawa, A theory of long-period magnetic pulsations, 1, Steady state excitation of field line resonance, *J. Geophys. Res., 79,* 1024, 1974.

Edwin, P. M., B. Roberts, and W. J. Hughes, Dispersive ducting of MHD waves in the plasma sheet: A source of Pi2 wave bursts, *Geophys. Res. Lett., 13,* 373–376, 1986.

Elphinstone, R. D., D. J. Hearn, L. L. Cogger, J. S. Murphree, A. N. Wright, I. Sandahl, S. Ohtani, P. T. Newell, D. M. Klumpar, M. Shapshak, T. A. Potemra, K. Mursula, and J. A. Sauvaud, The double oval UV auroral distribution 2. The most poleward arc system and the dynamics of the magnetotail, *J. Geophys. Res., 100,* 12,093–12,102, 1995.

Hansen, P. J., and B. G. Harrold, Parallel inhomogeneity and the Alfvén resonance, 1, Open field lines, *J. Geophys. Res., 99,* 2429, 1994.

Hopcraft, K. I., and P. R. Smith, Magnetohydrodynamic waves in a neutral sheet, *Planet. Space Sci., 34,* 1253, 1986.

Liu, W. W., B.-L. Xu, J. C. Samson, and G. Rostoker, Theory and observations of auroral substorms: A magnetohydrodynamic approach, *J. Geophys. Res., 100,* 79, 1995.

Mann, I. R., A. N. Wright, and P. S. Cally, Coupling of magnetospheric cavity modes to field line resonances: A study of resonance widths, *J. Geophys. Res., 100,* 19,441, 1995.

Seboldt, W., Nonlocal analysis of low-frequency waves in the plasma sheet, *J. Geophys. Res., 95,* 10,471, 1990.

Southwood, D. J., Some features of field line resonances in the magnetosphere, *Planet. Space Sci., 22,* 483, 1974.

Thompson, M. J., and A. N. Wright, Resonant Alfvén wave excitation in two-dimensional systems: Singularities in partial differential equations, *J. Geophys. Res., 98,* 15,551, 1993.

A. R. Garman and A. N. Wright, Department of Mathematical and Computational Sciences, University of St. Andrews, St. Andrews, Fife KY16 9SS, Scotland, U.K.

(Received June 11, 1997; revised September 29, 1997; accepted September 30, 1997.)